Graphical Abstract

Air-Carbon Ablation Model for Hypersonic Flight from Molecular Beam Data

Krishna Sandeep Prata, Thomas E. Schwartzentruber, Timothy K. Minton

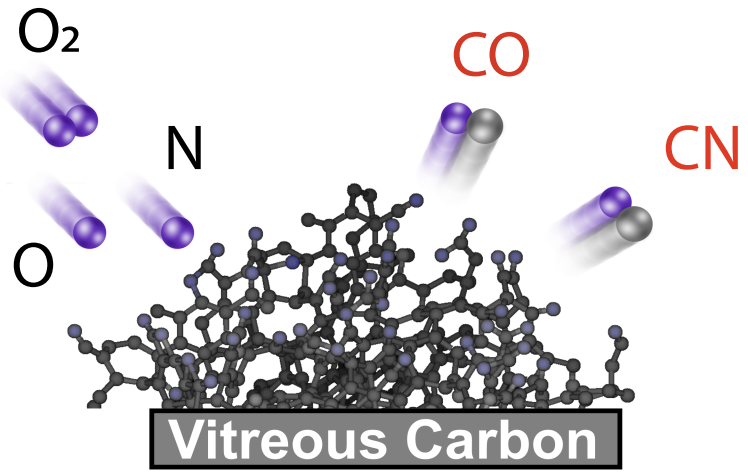

Highlights

Air-Carbon Ablation Model for Hypersonic Flight from Molecular Beam Data

Krishna Sandeep Prata, Thomas E. Schwartzentruber, Timothy K. Minton

- Research highlight 1
- Research highlight 2

Air-Carbon Ablation Model for Hypersonic Flight from Molecular Beam Data

Krishna Sandeep Prata[a,1,*], Thomas E. Schwartzentruber[a,2], Timothy K. Minton[b,3]

[a] *Department of Aerospace Engineering and Mechanics, University of Minnesota, Minneapolis, MN, 55414*
[b] *Ann and H.J. Smead Department of Aerospace Engineering Sciences, University of Colorado, Boulder, CO 80303*

Abstract

Recent molecular beam experiments of high velocity O, N, and O_2 impacting carbon material at high temperature produced detailed surface chemistry data relevant for carbon ablation processes. New data on O and N reactions with carbon has been published using a continuous molecular beam with lower velocity (2000 m/s) and approximately 500 times higher beam flux than previous pulsed-beam experiments. This data is interpreted to construct a new air-carbon ablation model for use in modeling carbon heat shield ablation. The new model comprises 20 reaction mechanisms describing reactions between impinging O, N, and O_2 species with carbon and producing scattered products including desorbed O and N, O_2 and N_2 formed by surface-catalyzed recombination, as well as CO, CO_2, and CN. The new model includes surface-coverage dependent reactions and exhibits non-Arrhenius reaction probabil-

*Corresponding author
[1]Graduate Research Assistant, Email: prata010@umn.edu
[2]Professor, Email: schwart@umn.edu
[3]Professor, Email: tminton@colorado.edu

ity in agreement with experimental observations. All reaction mechanisms and rate coefficients are described in detail and each is supported by experimental evidence or theory. The model predicts pressure effects and is tested for a wide range of temperatures and pressures relevant to hypersonic flight. Model results are shown to agree well with available data and are shown to have significant differences compared to other models from the literature.
Keywords: Ablation, Carbon oxidation, Carbon nitridation, Molecular Beam Experiments, Gas-surface interactions

---

1. Nomenclature

A_v	=	Avogadro number
B	=	Total active site density
E	=	Energy
F	=	One-fourth the mean thermal speed of a gas species
f	=	Flux of a species
k	=	rate coefficient
G	=	Subscript indicating gas
h	=	Planck's constant
k_b	=	Boltzmann constant
m	=	Mass of an atom of a species
N	=	Subscript for atomic nitrogen
O	=	Subscript for atomic oxygen
ox	=	Subscript for molecular oxygen
P	=	Partial pressure
p	=	Probability

R = Universal gas constant

S = Adsorption selectivity

T = Temperature

2. Introduction

Hypersonic vehicles create strong shock waves, and associated high temperatures, that partially dissociate the surrounding air. Due to high flow speeds, the gas near the vehicle surface remains in chemical nonequilibrium and reactive atomic species (O and N atoms) reach the vehicle surface and damage the heat shield. New hypersonic mission trajectories involve sustained flight under nonequilibrium conditions where the gas-surface chemistry requires finite-rate modeling. The complexity increases dramatically in the case of finite-rate modeling compared to equilibrium gas-surface chemistry modeling. Finite-rate models require the specification of many surface chemistry mechanisms and accompanying rate coefficients, most of which are not well understood or measurable experimentally.

This article focuses on gas-surface reaction modeling for carbon, often used for ablative heat shields. Two models that have been used in the recent literature include the Park model [1] and the Zhluktov and Abe (ZA) model [2]. Experimental validation of gas-surface reaction models has proven to be challenging. Both models were used to compare computations to experimental data from the passive ablation nose-tip technology (PANT) configuration [3][4], and both models under-predicted the stagnation point ablative mass flux, under high pressure conditions. Gosse and Candler [5] added new sublimation reactions to the Park model, however, the stagnation temperature and

recession rates were still under-predicted when compared to the PANT data. MacLean et al. [6] compared four different models (two models based on the work of Park, the ZA model, and a constant oxidation probability model) and found that all four models predicted different recession rates. Candler [7] performed a numerical analysis of the ZA and Park models, in addition to the equilibrium B' model, for hypersonic conditions, between 20 and 40 km altitude, and found significant differences between model predictions. Lewis et al. [8][9] performed a series of hypersonic ablation experiments in the X-2 facility at the University of Queensland, and CFD simulations comparing the Park and ZA models were performed by Alba et al. [10][11]. In these cases, the surface temperature ranged from 1770 to 2410 K. The predicted ablation products were quite different between the Park and ZA models, and neither of the models was able to predict the experimentally observed products. The challenge in using high enthalpy experiments (such as arc-jets or inductively coupled plasma (ICP) facilities) for model development is that measured surface recession, heat flux, and species concentrations in the boundary layer, are the net result of many gas-surface and gas-phase reaction mechanisms. It is difficult to choose reaction mechanisms and set all of the free parameters using such data, and typically there are many combinations of reaction mechanisms and rate coefficients that may reproduce macroscopic measurements, such as heat flux or surface recession, for a given experiment. Model accuracy for conditions outside of the experimental conditions is therefore uncertain.

Recently, new surface chemistry data was obtained in molecular beam-surface scattering experiments on carbon over a wide range of high tem-

peratures [12][13]. The experiments involved a pulsed beam of atomic and molecular oxygen, traveling at a nominal velocity of 7756 m/s, and impacting a vitreous carbon (VC) surface that was resistively heated to high temperatures. This hyperthermal beam was pulsed at a repetition rate of 2 Hz and was composed of 93% atomic and 7% molecular oxygen. The average translational energies of the atomic and molecular components of the beam were 4.99 and 9.98 eV, respectively, with energy widths (full width at half-maximum) of 0.57 and 1.66 eV, respectively. Both atomic and molecular oxygen were in their ground electronic states [14][15]. The general experimental setup [12][16][17] includes a rotatable mass spectrometer to monitor both the incident molecular beam and the volatile species that scatter from the surface. Experiments were performed at various surface temperatures for VC samples[12][13], and further experiments were performed for highly oriented pyrolytic graphite (HOPG) samples [18], and FiberForm samples [19]. The experiments provided a wealth of data regarding what reactions were dominant and the reaction probabilities for different products leaving the surface. This data was used to construct a probability model for use in direct simulation Monte Carlo (DSMC) [20] and a finite-rate model for use in computational fluid dynamics (CFD) [21].

In this article, we extend this model to air-carbon reactions and include reactions due to O, O_2, and N (N_2 is assumed to be inert) collisions. Recently new campaigns of molecular beam experiments were carried out using O, N, and mixed O/N beams impacting VC samples. Experiments that used the mixed O/N beam used a pulsed incident beam [22]. The recent experiments that examined the individual interactions of O or N atoms with a VC surface

used a different beam source that operated continuously (not pulsed like prior experiments) with lower-velocity reactants impacting the material [23]. The continuous O-atom beam results reveal similar trends as the original pulsed beam results. This lends strong support to the assumptions and conclusions drawn in the previous modeling studies [20][21]. Since data is now available for O atoms, N atoms, a mixture of O and N atoms, along with separate data on O_2 collisions with carbon [24][25][26], we are able to construct an air-carbon ablation model, as described in this article.

3. New Molecular Beam Data and Relevance to Hypersonic Ablation

The previous pulsed molecular beam experiments on oxygen interacting with vitreous carbon [12] revealed four general results directly relevant to ablation processes under hypersonic conditions. First, reaction products scattered thermally (accommodated to the surface temperature), despite the high incident energy of the reactants. This result implied that the beam energy and angle has no effect on the surface chemistry; rather, the beam simply acts as a supply of oxygen atoms to the surface and the material temperature is the dominant parameter controlling the reaction probability. Second, the rotatable mass spectrometer was able to clearly differentiate between individual reaction efficiencies. For example, CO was the dominant product at all temperatures, and CO_2 was a minor reaction product. Third, non-Arrhenius behavior was observed for the CO product formation. At temperatures between 800-1200 K, the probability of CO production increased with surface temperature. However, above approximately 1200 K, CO production was

observed to decrease while the O-atom flux leaving the surface markedly began to increase (indicating a decrease in surface or subsurface oxygen content). Therefore, despite the low pressure environment (near-vacuum) of the molecular beam experiments, the collected data spanned regimes of high surface coverage and the transition to low surface coverage. Fourth, molecular beam experiments were performed on three types of carbon surfaces: highly-oriented pyrolytic graphite (HOPG) [18], vitreous carbon (VC) [12], and FiberForm [19]. The main trends discussed above were consistent across each material, indicating that the measurements were general to many ablating carbon materials (i.e., those with significant roughness at the micron-scale and highly defected atomistic surface morphology). Each of these four key results supported the premise that molecular beam experiments may provide relevant data for modeling carbon ablation occurring in the presence of a hypersonic boundary layer.

However, certain assumptions were required in prior modeling efforts that led to some level of uncertainty in interpreting the experimental measurements and incorporating them into hypersonic ablation models. Specifically, although reaction products scattered thermally, it could be possible that the high beam energy and low atomic oxygen flux, compared to that from a boundary layer gas, produces different surface chemistry than would be expected in an actual hypersonic boundary layer. Furthermore, the pulsed nature of the molecular beam led to in-depth studies of the time-varying aspects of the experiments [27][28]. In contrast, the original model by Poovathingal et al. [20][21], assumed that the reaction products (and their relative probabilities) observed during the beam pulse would be the same as

those observed if the beam were continuously operating, and the unsteady details of the measurements between pulses were not relevant to formulate an ablation model. It was also observed experimentally that the product flux (leaving the surface) captured by the mass spectrometer was not the same at high and low temperatures, despite the same molecular beam conditions (i.e., the same beam flux). Since reaction products were observed to leave the surface thermally, the model by Poovathingal et al. [20][21] assumed that the product flux not captured by the detector had similar chemical composition as the product flux that was captured by the detector. In contrast, the model by Swaminathan-Gopalan et al. [27] assumed that the product flux not captured by the detector was entirely composed of CO and that this CO was not counted because it left the surface *between* beam pulses. Finally, a hysteresis effect was observed in the pulsed beam experiments where the measured reaction probabilities differed as the material sample was being slowly heated (over several hours) compared to when the sample was being slowly cooled, for the same temperature when a measurement was taken. This led to uncertainty in which value of reaction probability should be used for a given material temperature, and raised the possibility that perhaps the hysteresis itself needed to be modeled.

To address these uncertainties and to provide a larger set of experimental data, new molecular beam experiments were recently performed [23]. The new experiments involved continuous beams containing O or N atoms with incident velocities of approximately 2000 m/s, which were directed at a vitreous carbon (VC) surface at temperatures ranging from 800 – 1873 K. Furthermore, the incident O- or N-atom flux in the new experiments was up to

three orders of magnitude higher than the fluxes used in the earlier studies with the hyperthermal pulsed beams. A hysteresis effect was also observed in the new experiments; however it was clearly less pronounced than in the pulsed beam studies and the difference in inferred reaction probability due to the hysteresis effect was only slightly larger than the uncertainty in the reaction probability itself. Therefore the new, continuous, lower velocity, and higher flux, molecular beam experiments were able to address the main assumptions and uncertainties from the previous pulsed beam experiments. As described in detail in Ref. [23], despite significant differences between the new continuous beam experiments and the earlier pulsed beam experiments, the results are remarkably similar. Similar to the pulsed beam experiments, the new continuous beam experiments also observed a difference in product flux (leaving the surface) captured by the mass spectrometer at high versus low temperatures [23]. If the missing flux were comprised entirely of CO products leaving the surface at longer timescales between beam pulses (as proposed by Swaminathan-Gopalan et al. [27]), then such CO products would have been measured in the continuous beam/detector experiments, and should have significantly changed the measured CO trend with temperature. The new experiments showed no such change in CO flux behavior compared to the original pulsed beam experiments. In fact, each of the four general results discussed above was also observed in the new experiments (including atomic force micrograph analysis of the micron-level surface morphology), and therefore the new experiments corroborated the thermal gas-surface interaction mechanisms inferred from earlier studies as well as the assumptions made in interpreting the data [20][21]. In addition, the new experiments included

exposure of VC samples to beams containing N and N_2, and also revealed the probabilities of N-atom and O-atom surface recombination reactions to form gas-phase N_2 and O_2 molecules.

The results of the new molecular beam experiments are fully described in Ref .[23], and will be presented along with model results later in Section 5. Before constructing the new finite-rate air-carbon ablation model, it is useful to first summarize the main experimental findings. The new continuous molecular beam experiments expose a partially ablated, high temperature, VC carbon sample to a continuous flux of O or N atoms at velocities comparable to the mean thermal speed of atomic species in a hypersonic boundary layer ($\approx$ 2000 m/s). Under such conditions, all reactions proceed thermally and products leave the surface accommodated to the carbon surface temperature. The rotatable mass spectrometer is able to quantify the efficiencies of individual gas-surface interactions, both reactive and non-reactive, as a function of the surface temperature. Reactions forming CO (the dominant product) are surface-coverage dependent reactions that exhibit non-Arrhenius rate behavior at high surface temperature where surface coverage is reduced due to the desorption of O atoms. Reactions forming CO_2 (minor product) are found to have reduced probabilities as temperature is increased and are not measurable above a certain threshold temperature. In addition to the oxidation reactions producing CO and CO_2, oxygen atoms are observed to recombine on the surface to produce gas-phase O_2 with an efficiency that is lower than that of CO production, but not negligible. Nitrogen atoms may recombine on the surface to produce gas-phase N_2 or react to produce CN, and importantly, the recombination efficiency of N atoms

was found to be more than an order of magnitude higher than the reaction efficiency to produce CN. In addition to this wealth of new experimental data, additional molecular beam data for O_2 interacting with carbon has recently been reported [24] and can be combined with legacy experimental O_2 carbon measurements [25][26]. Finally, new experiments where molecular beams containing a *mixture* of N and O atoms interacting with hot VC samples have been performed [22], which provide valuable information about if, and how, N and O atoms compete for surface coverage and indirectly influence oxidation reactions. Unfortunately, these experiments did not address the possibility that NO may be formed on a carbon surface that is simultaneously bombarded by O and N atoms. Nevertheless, new molecular dynamics simulations of N atoms reacting with oxygen defects on a graphene surface suggest that NO formation may not be important at incident velocities relevant to gas-surface interactions in a hypersonic shock layer[29]. By combining the consistent results of the original high-velocity pulsed molecular beam data with the new lower-velocity continuous beam data, along with the new mixed beam data, we now have sufficient experimental data for oxygen and nitrogen interactions with carbon in order to extend the previous oxygen-carbon model [21] to a new finite-rate *air*-carbon ablation model.

The purpose of this article is to describe how the molecular beam data is used to construct the new air-carbon reaction model and to clearly describe the rationale behind the choices of reaction mechanisms and the values of model parameters. Model simplifications are also discussed and model trends are tested over a wide range of temperatures and pressures and compared with available data. Ultimately, the model requires validation within CFD

simulations of high-enthalpy ablation experiments; however, this is beyond the scope of the current article. Among other challenges, the validation of ablation models with measurements from high-enthalpy experiments requires accurate characterization of the free-stream plasma conditions; an active area of on-going research.

4. Model Description

The previous oxygen-carbon reaction model of Poovathingal et al. [21] consisted of five reaction mechanisms: (i) adsorption of O, (ii) desorption of O, (iii) CO formation dependent on adsorbed O, (iv) CO_2 formation dependent on adsorbed O, and (v) direct CO formation independent of adsorbed O. The fifth reaction was added to maintain CO production even at high temperatures where surface coverage was very low and, as noted in that prior work [21], is not a physically realistic reaction mechanism. In both the original pulsed molecular beam data and the new continuous molecular beam data, there is evidence of a slower surface-mediated reaction, which may involve a different "type" of adsorbed O. Therefore, we start by eliminating the fifth reaction and instead we include two types of adsorbed oxygen in our new model. Furthermore, recombination of O atoms into O_2 molecules was also observed in the new experiments and recombination reactions are therefore added to the model. Nitrogen reactions including N adsorption, N desorption, formation of CN, and surface recombination into N_2, are added to the model based on the new nitrogen molecular beam data. It is important to note that the addition of recombination reactions has significant implications for the overall model, since recombination reactions now compete with oxi-

dation and nitridation reactions. Finally, data for O_2 collisions with carbon are also incorporated into the model.

The new air-carbon ablation model contains 20 reactions. Each reaction rate expression has a physics-based functional form and the selection of model parameters is supported by experimental data and/or theory. To begin, we present the full reaction model and clearly describe each reaction rate expression. It is important to note that we first present the model without discussion and justification for each reaction. Only in section 5, after the model has been presented, do we compare model results with experimental data, at which point, we present detailed discussion and justification for each mechanism and rate expression. In the process, we present model results over a wide range of temperatures and pressures and compare to the molecular beam data and also to reaction probabilities inferred from inductively coupled plasma (ICP) testing facilities.

4.1. General Description of the model

One general reaction mechanism we desire to model is when the gas-phase reactant first adsorbs on to the surface before forming a product through gas-surface interaction. The rate of adsorption of a gas-phase reactant G (G is O, N, or O_2 in the current model) is $k_{ad}[G][(s)]$, where k_{ad} is the rate coefficient, [G] is the concentration of the gas-phase species (in mol m^{-3}), and [(s)] is the surface density of the empty reactive sites (in mol m^{-2}). The rate coefficient k_{ad} depends on the mean thermal speed of the gas species, the selectivity of absorption (S), the total active site density B (in mol m^{-2}), and the activation energy for adsorption (E_{ad}) as shown in Eq. (1). The selectivity of adsorption lies between 0 and 1.

$$k_{ad} = \frac{1}{B} * F_G * S * \exp \frac{-E_{ad}}{RT} \tag{1}$$

The flux of gas species to the surface ($f_{G,in}$) is $F_G[G]$, where F_G is one-fourth the mean thermal speed of the gas species given by Eq. (2).

$$F_G = \frac{1}{4}\sqrt{\frac{8k_bT}{\pi m_G}} \tag{2}$$

The adsorbed species G(s) desorbs from the surface with a rate equal to $k_{des}[G(s)]$, where [G(s)] is the surface density of the adsorbed species (in mol m^{-2}). The desorption rate coefficient k_{des} is modeled according to the simple transition state theory assumption, with a desorption energy of E_{des} and is given by Eq. (3).

$$k_{des} = \frac{2\pi m_G k_b T^2}{A_v B h^3} \exp \frac{-E_{des}}{RT} \tag{3}$$

The reactions that produce gas-phase products are of two types - reactions that remove a carbon atom from the surface, and surface-catalyzed recombination reactions. The carbon removing reactions can either be gas-phase dependent or gas-phase independent. The rate of a gas-phase dependent reaction is equal to $k_{gd}[G][G(s)]$, where k_{gd} is the rate coefficient that depends on the kinetic-flux of the gas-phase reactant, and the probability of the reaction (p_{gd}), and is given by Eq. (4).

$$k_{gd} = F_G * p_{gd} \tag{4}$$

The rate of gas-phase independent reactions is given by $k_{gi}[G(s)]$, where k_{gi} is the reaction rate coefficient. The rate coefficient k_{gi} takes a simple

Arrhenius form. Recombination reactions can be either gas-phase dependent (often referred to as Eley-Rideal or ER) reactions or gas-phase independent (often referred to as Langmuir-Hinshelwood or LH) reactions. The rate of an ER reaction is given by $k_{er}[G][G(s)]$, where the reaction rate coefficient k_{er} is given by Eq. (5). The pre-exponential factor γ_{er} takes a value between 0 and 1.

$$k_{er} = \frac{1}{B} * F_G * \gamma_{er} * \exp \frac{-E_{er}}{RT} \tag{5}$$

The rate of an LH recombination mechanism is given by $k_{lh}[G(s)][G(s)]$, where the rate coefficient k_{lh} is given by Eq. 6. The pre-exponential factor γ_{lh} takes a value between 0 and 1. A_v is the Avogadro number, and $F_{G,2D}$ is the mean thermal speed of the mobile adsorbed species on the surface, given by Eq. 7.

$$k_{lh} = \sqrt{\frac{A_v}{B}} * F_{G,2D} * \gamma_{lh} * \exp \frac{-E_{lh}}{RT} \tag{6}$$

$$F_{G,2D} = \sqrt{\frac{\pi k_b T}{2 m_G}} \tag{7}$$

The functional forms of the reaction rates and rate coefficients described above are standard forms used by previous researchers and, for example, a more detailed description can be found in Chapter 6 of Ref. [30]. Table 1 contains the new model chemical reaction mechanisms, the reaction rates, and the rate coefficients. The model contains 20 reactions, describing oxidation by atomic and molecular oxygen, nitridation by atomic nitrogen, and surface catalyzed recombination of both atomic nitrogen and atomic oxygen.

The actual reactions between O or N atoms and carbon, especially highly defected carbon, are undoubtedly more complicated than those used in the model. The reactions in the model have been chosen to represent classes of reactions that lead to the products with distinguishing dynamical characteristics that have been experimentally observed. We first present a full description of the model and parameter values, and later in section 5, we describe the rationale behind the choice of reaction mechanisms and parameter values while comparing to experimentally inferred reaction probabilities.

Table 1: Reaction mechanisms

R.No	Reaction	Reaction Rate	Rate Coefficient	Units
1.	$O + (s) \rightarrow O(s)$	$k_{O1}[O][(s)]$	$\frac{F_O}{B} * 0.3$	$m^3 mol^{-1} s^{-1}$
2.	$O(s) \rightarrow O + (s)$	$k_{O2}[O(s)]$	$\frac{2\pi m_O k_b^2 T^2}{A_v B h^3} \exp \frac{-44277}{T}$	s^{-1}
3.	$O + O(s) + C(b) \rightarrow CO + O + (s)$	$k_{O3}[O][O(s)]$	$\frac{F_O}{B} 100 \exp \frac{-4000}{T}$	$m^3 mol^{-1} s^{-1}$
4.	$O + O(s) + C(b) \rightarrow CO_2 + (s)$	$k_{O4}[O][O(s)]$	$\frac{F_O}{B} \exp \frac{-500}{T}$	$m^3 mol^{-1} s^{-1}$
5.	$O + (s) \rightarrow O^*(s)$	$k_{O5}[O][(s)]$	$\frac{F_O}{B} * 0.7$	$m^3 mol^{-1} s^{-1}$
6.	$O^*(s) \rightarrow O + (s)$	$k_{O6}[O^*(s)]$	$\frac{2\pi m_O k_b^2 T^2}{A_v B h^3} \exp \frac{-96500}{T}$	s^{-1}
7.	$O + O^*(s) + C(b) \rightarrow CO + O + (s)$	$k_{O7}[O][O^*(s)]$	$\frac{F_O}{B} 1000 \exp \frac{-4000}{T}$	$m^3 mol^{-1} s^{-1}$
8.	$O^*(s) + O^*(s) \rightarrow O_2 + 2(s)$	$k_{O8}[O^*(s)]^2$	$\sqrt{\frac{A_v}{B}} F_{O,2D} * 1 * 10^{-3} \exp \frac{-15000}{T}$	$m^2 mol^{-1} s^{-1}$
9.	$O(s) + O(s) \rightarrow O_2 + 2(s)$	$k_{O9}[O(s)]^2$	$\sqrt{\frac{A_v}{B}} F_{O,2D} 5 * 10^{-5} \exp \frac{-15000}{T}$	$m^2 mol^{-1} s^{-1}$

10.	$N + (s) \rightarrow N(s)$	$k_{N1}[N][(s)]$	$\frac{F_N}{B} \exp \frac{-2500}{T}$	$m^3 mol^{-1} s^{-1}$
11.	$N(s) \rightarrow N + (s)$	$k_{N2}[N(s)]$	$\frac{2\pi m_N k_b^2 T^2}{A_v B h^3} \exp \frac{-73971}{T}$	s^{-1}
12.	$N + N(s) + C(b) \rightarrow CN + N + (s)$	$k_{N3}[N][N(s)]$	$\frac{F_N}{B} 1.5 \exp \frac{-7000}{T}$	$m^3 mol^{-1} s^{-1}$
13.	$N + N(s) \rightarrow N_2 + (s)$	$k_{N4}[N][N(s)]$	$\frac{F_N}{B} 0.5 \exp \frac{-2000}{T}$	$m^3 mol^{-1} s^{-1}$
14.	$N(s) + N(s) \rightarrow N_2 + 2(s)$	$k_{N5}[N(s)]^2$	$\sqrt{\frac{A_v}{B}} F_{N,2D} 0.1 \exp \frac{-21000}{T}$	$m^2 mol^{-1} s^{-1}$
15.	$N(s) + C(b) \rightarrow CN + (s)$	$k_{N6}[N(s)]$	$1e + 08 \exp \frac{-20676}{T}$	s^{-1}
16.	$O_2 + 2(s) \rightarrow 2O(s)$	$k_{ox1}[O_2][(s)]^2$	$\frac{F_{O_2}}{B^2} 1 \exp \frac{-8000}{T}$	$m^5 mol^{-2} s^{-1}$
17.	$O_2 + O(s) + C(b) \rightarrow CO + O_2 + (s)$	$k_{ox2}[O_2][O(s)]$	$\frac{F_{O_2}}{B} 100 \exp \frac{-4000}{T}$	$m^3 mol^{-1} s^{-1}$
18.	$O_2 + O(s) + C(b) \rightarrow CO_2 + O + (s)$	$k_{ox3}[O_2][O(s)]$	$\frac{F_{O_2}}{B} 1 \exp \frac{-500}{T}$	$m^3 mol^{-1} s^{-1}$
19.	$O_2 + 2(s) \rightarrow 2O^*(s)$	$k_{ox4}[O_2][(s)]^2$	$\frac{F_{O_2}}{B^2} 1 \exp \frac{-8000}{T}$	$m^5 mol^{-2} s^{-1}$
20.	$O_2 + O^*(s) + C(b) \rightarrow CO + O_2 + (s)$	$k_{ox5}[O_2][O^*(s)]$	$\frac{F_{O_2}}{B} 1000 \exp \frac{-4000}{T}$	$m^3 mol^{-1} s^{-1}$

4.2. Reactions involving atomic oxygen (O)

Reactions involving atomic oxygen are given by reactions (1) – (9). We propose that there are two types of adsorbed oxygen, a relatively weakly bound O(s) and a relatively strongly bound O^*(s). Reactions (1) and (5) are the adsorption reactions for O into O(s) and O^*(s), respectively. The selectivity of adsorption of O into O(s) is 0.3 and into O^*(s) is 0.7, with a combined adsorption selectivity of 1. The adsorption is prompt in that there is no activation energy barrier. The desorption of O(s) and O^*(s) into O are given by reactions (2) and (6), respectively, with simple transition state theory based reaction constants. However, O(s) desorbs more readily than O^*(s) since the desorption energy for O(s) is $\sim$ 245 kJ/mol (equal to the bond energy of a single bond between C and O) while that for O^*(s) is $\sim$ 800 kJ/mol (equal to the bond energy of a double bond between C and O). Reactions (3) and (7) are the gas-phase dependent reactions forming CO through O(s) and O^*(s) respectively. The activation energy and the pre-exponential factors are chosen to capture the trends of the experimental data. Modeling CO formation with a gas-phase dependent mechanism is important for model accuracy at high pressures, for example, similar gas-phase dependent reactions were used in the model by Poovathingal et al. [21]. Reaction (4) is the gas-phase dependent CO_2 formation mechanism dependent on O(s). We choose not to have an O^*(s) dependent CO_2 formation mechanism for simplicity, and because CO_2 production vanishes at higher temperatures in the experiments, which is where O^*(s) persists. Reactions (8) and (9) are the LH recombination reactions through O^*(s) and O(s) respectively into gas-phase O_2. The activation energy of both the reactions is the same and is chosen to

best match the slope observed in the experimental data.

4.3. Reactions involving atomic nitrogen (N)

Reactions involving atomic nitrogen are given by reactions (10) - (15). We model only one type of adsorbed nitrogen, N(s). Reaction (10) is the adsorption of N into N(s). The adsorption of N is not prompt unlike the adsorption of O, but is activated, with an energy barrier of about 21 kJ/mol. The reason for an activated N adsorption will be discussed in section 5, when we present comparisons with experimental data. Reaction (11) is the desorption of N(s) into N and has a transition state theory based rate coefficient with a desorption energy of ∼615 kJ/mol, equivalent to the bond energy of a double bond between C and N. This choice will be discussed further in section 5. For nitridation, we propose two CN formation reactions – one gas-phase dependent and the other gas-phase independent. Reaction (12) is the gas-phase dependent CN formation mechanism, necessary for model accuracy at high pressures. The activation energy of the gas-phase dependent CN formation reaction is chosen to match the CN probability inferred from high pressure inductively coupled plasma (ICP) ablation testing facilities. Reaction (15) is the C-CN bond cleavage mechanism, postulated in the new molecular beam experimental analysis [23]. This reaction mechanism enables the model to capture significantly different CN formation probabilities reported over a wide range of pressure, and will be discussed further in section 5. The activation energy for this reaction is determined by the molecular beam experiments. Finally, reaction (13) is the ER recombination reaction producing N_2 and reaction (14) is the LH recombination of N(s) into N_2. Although the molecular beam experiments (near-vacuum condi-

tions) showed evidence of only LH-type recombination, we find that both types of recombination reactions are necessary to match measured recombination probabilities reported over a wide range of pressures. This is described in more detail in section 5.

4.4. Reactions involving molecular oxygen (O_2)

Molecular oxygen reacts with carbon through reactions similar to those of atomic oxygen. The difference lies in how O_2 adsorbs onto the surface. Molecular oxygen adsorbs onto carbon through dissociative chemisorption in which O_2 can partially chemisorb onto the surface or fully chemisorb onto the surface. When fully chemisorbed, the molecule dissociates and two adsorbed oxygen atoms are formed. When partially chemisorbed, the molecule dissociates forming one adsorbed oxygen atom and one gas phase oxygen atom. Since O_2 must dissociate to chemisorb, the chemisorption is not prompt, but rather is activated. Reactions (16) and (19) are the fully dissociative chemisorption reactions of O_2. Once chemisorbed, O_2 reacts with precisely the same mechanisms as atomic oxygen does – forming CO and CO_2 through gas-phase dependent reactions (17), (18), and (20). The reaction rate coefficients for these reactions are therefore set equal to those of the corresponding reactions involving O.

4.5. Zero-dimensional (0D) simulation procedure

The reaction mechanisms and rates in Table I can be used to simulate a zero-dimensional (0D) system in which a set of ordinary differential equations (ODEs) are integrated in time to obtain product fluxes. Inputs to the 0D simulations include the gas composition (concentrations and partial pressures

of each species) next to the surface and the temperature of the gas next to the surface, which is equal to the surface temperature (T). The partial pressures and gas temperature simply set the flux of species to the surface via the reaction rates and Eq. 2, for example. In the current model, the total active site density is set as, $B = 1 \times 10^{-5}$ mol m^{-2}. This is the same value used in the work of Poovathingal et al. [20][21] and is similar to the value used in the ZA model [2]. Further discussion of this parameter is presented in subsection 5 of section 5. Given the partial pressures and gas-surface temperature, combined with the reaction rate expressions and model parameters, and given an initial surface coverage (O(s), O*(s), and N(s) at $t = 0$), a set of ODEs can be integrated in time to predict the evolution of surface coverage and product fluxes leaving the surface. For much of our analysis, a steady-state surface coverage, and corresponding steady-state product flux, is reached quickly and we therefore focus mainly on steady-state results.

In addition to plotting model results for general temperature and pressure (T, P) gas conditions, we also plot model results corresponding to molecular beam experimental conditions. In this case, what matters is that the flux of species to the surface in the 0D simulation matches the actual flux of species to the surface in the molecular beam experiment. Both temperature and pressure are not well defined in the molecular beam, nor near the surface in the molecular beam experiment, due to the free-molecular nature of the gas-surface interaction. Since the input (T, P) values are only used indirectly to determine the kinetic flux to the surface, we simply impose $P_{beam} = 2.4 \times 10^{-2}$ Pa and $T_{beam} = 1000$ K. The partial pressures of the species and the temperature set the molar concentrations, [G], through the ideal gas law.

This results in a simulated flux equal to 5×10^{20} atoms m^{-2} s^{-1}, which matches the beam flux in the experiments. Note that this flux is kept constant for all plotted molecular beam results, while the surface temperature (T) is varied, since the molecular beam flux was always constant no matter what temperature the VC material was.

The following system of ordinary differential equations (ODEs) is obtained through the reaction mechanisms in Table I:

$$\begin{aligned}\frac{d[O(s)]}{dt} &= k_{O1}[O][(s)] - k_{O2}[O(s)] - k_{O3}[O][O(s)] - k_{O4}[O][O(s)] \\ &\quad - 2k_{O9}[O(s)]^2 + 2k_{ox1}[O_2][(s)]^2 - k_{ox2}[O_2][O(s)] - k_{ox3}[O_2][O(s)]\end{aligned} \tag{8}$$

$$\begin{aligned}\frac{d[O^*(s)]}{dt} &= k_{O5}[O][(s)] - k_{O6}[O^*(s)] - k_{O7}[O][O^*(s)] - 2k_{O8}[O^*(s)]^2 \\ &\quad + 2k_{ox4}[O_2][(s)]^2 - k_{ox5}[O_2][O^*(s)]\end{aligned} \tag{9}$$

$$\begin{aligned}f_{CO} = \frac{d[CO]}{dt} &= k_{O3}[O][O(s)] + k_{O7}[O][O^*(s)] + k_{ox2}[O_2][O(s)] \\ &\quad + k_{ox5}[O_2][O^*(s)]\end{aligned} \tag{10}$$

$$f_{CO_2} = \frac{d[CO_2]}{dt} = k_{O4}[O][O(s)] + k_{ox3}[O_2][O(s)] \tag{11}$$

$$\begin{aligned}f_O = \frac{d[O]}{dt} &= \frac{P_O}{A_v\sqrt{2\pi m_O k_b T}} - k_{O1}[O][(s)] + k_{O2}[O(s)] - k_{O4}[O][O(s)] \\ &\quad - k_{O5}[O][(s)] + k_{O6}[O^*(s)] + k_{ox3}[O_2][O(s)]\end{aligned} \tag{12}$$

$$f_{O_2} = \frac{d[O_2]}{dt} = \frac{P_{O_2}}{A_v\sqrt{2\pi m_{O_2} k_b T}} + k_{O8}[O^*(s)]^2 + k_{O9}[O(s)]^2 - k_{ox1}[O_2][(s)]^2 - k_{ox3}[O_2][O(s)] - k_{ox4}[O_2][(s)]^2 \tag{13}$$

$$\frac{d[N(s)]}{dt} = k_{N1}[N][(s)] - k_{N2}[N(s)] - k_{N3}[N][N(s)] - k_{N4}[N][N(s)] - 2k_{N5}[N(s)]^2 - k_{N6}[N(s)] \tag{14}$$

$$f_{CN} = \frac{d[CN]}{dt} = k_{N3}[N][N(s)] + k_{N6}[N(s)] \tag{15}$$

$$f_N = \frac{d[N]}{dt} = \frac{P_N}{A_v\sqrt{2\pi m_N k_b T}} - k_{N1}[N][(s)] + k_{N2}[N(s)] - k_{N4}[N][N(s)] \tag{16}$$

$$f_{N_2} = \frac{d[N_2]}{dt} = k_{N4}[N][N(s)] + k_{N5}[N(s)]^2 \tag{17}$$

Since the total active site density, B is constant, the following equation must be satisfied:

$$[O(s)] + [O^*(s)] + [N(s)] + [(s)] = B \tag{18}$$

If desired, the system of ODEs can be integrated in time to provide the time-varying evolution of surface coverage and reaction products. We note that such unsteady analysis is *not* related to modeling of the transient processes inherent in the pulsed molecular beam studies. To be clear, our finite-rate model is not meant to precisely simulate the pulsed molecular beam experiments, as was done by Swaminathan-Gopalan et al. [27][28], because

the transient surface chemistry occurring *between* such beam pulses is not relevant for a hypersonic ablation model. In contrast, unsteady solution of our model equations would simulate the evolution of surface coverage and carbon reactivity when exposed to a continuous high-flux of species as produced by a hypersonic boundary layer. When we integrate our model equations to steady-state for a wide range of temperature, pressure, and composition conditions, we find that the maximum time required to reach steady-state is approximately 1 second of physical time for the molecular beam conditions (near vacuum) and 10^{-7} seconds for high pressures typical in ICP tests. To clarify, assuming steady-state does not imply chemical equilibrium, rather a steady-state assumption implies that the local surface coverage adapts "instantly" to the near-surface gas state, which itself may be time-varying and in a state of chemical nonequilibrium. Our model does not capture the temperature-dependent hysteresis observed in the experiments. However, as mentioned in section 3, the hysteresis effect was noticeably smaller in the new continuous beam experiments, and this uncertainty in reaction probability is comparable to the overall uncertainty introduced by other modeling assumptions. Furthermore, it is quite possible that such a hysteresis effect will not be present under gas pressures typical in a hypersonic boundary layer. Understanding the cause of the hysteresis in the beam experiments and modeling any potential effects for hypersonic boundary layer conditions is beyond the scope of this article.

If the steady-state surface coverage and reactant fluxes are of interest, then it is more computationally efficient to reduce the ODEs to the steady-state limit. A steady state solution can be obtained by setting the rate

of change in surface coverage equal to zero, i.e., $\frac{d[O(s)]}{dt} = \frac{d[O^*(s)]}{dt} = \frac{d[N(s)]}{dt} = 0$, and subsequently solving for the steady-state surface coverages while satisfying Eq. (18). The steady state equations can be rearranged in the following form:

$$\begin{aligned} A_1[(s)]^2 + B_1[(s)] &= C_1[O(s)]^2 + D_1[O(s)], \\ A_2[(s)]^2 + B_2[(s)] &= C_2[O^*(s)]^2 + D_2[O^*(s)], \\ A_3[(s)]^2 + B_3[(s)] &= C_3[N(s)]^2 + D_3[N(s)], \\ [O(s)] + [O^*(s)] + [N(s)] + [(s)] &= B. \end{aligned} \tag{19}$$

where

$$\begin{aligned} &A_1 = 2k_{Ox1}[O_2]; B_1 = k_{O1}[O]; \\ &C_1 = 2k_{o9}; D_1 = k_{O2} + (k_{O3} + k_{O4})[O] + (k_{ox2} + k_{ox3})[O_2] \\ &A_2 = 2k_{ox4}[O_2]; B_2 = k_{O5}[O]; \\ &C_2 = 2k_{O8}; D_2 = k_{O6} + k_{O7}[O] + k_{ox5}[O_2] \\ &A_3 = 0; B_3 = k_{N1}[N]; C_3 = 2k_{N5}; D_3 = k_{N2} + k_{N6} + (k_{N3} + k_{N4})[N] \end{aligned} \tag{20}$$

Without loss of generality, consider

$$A_1[(s)]^2 + B_1[(s)] = C_1[O(s)]^2 + D_1[O(s)].$$

Assuming that LHS is a constant, we can write an expression for [O(s)] using the alternative form of the quadratic formula:

$$[O(s)] = \frac{2(A_1[(s)]^2 + B_1[(s)])}{D_1 + \sqrt{D_1^2 + 4C_1(A_1[(s)]^2 + B_1[(s)])}}. \tag{21}$$

Similarly, we can write [O*(s)] and [N(s)] as shown in Eq. (22) and Eq. (23).

$$[O^*(s)] = \frac{2(A_2[(s)]^2 + B_2[(s)])}{D_2 + \sqrt{D_2^2 + 4C_2(A_2[(s)]^2 + B_2[(s)])}} \tag{22}$$

$$[N(s)] = \frac{B_3[(s)]}{D_3 + \sqrt{D_3^2 + 4C_3B_3[(s)]}} \tag{23}$$

Substituting Eq. (21), Eq. (22), and Eq. (23) into Eq. (18), we numerically calculate the steady-state surface density of empty sites using Eq. (24). Note that the alternative form of quadratic formula is used so that the current solution method can also be used when the quadratic terms on the RHS of the steady-state equations become zero – i.e., when no LH recombination mechanisms are present.

$$\begin{aligned}[(s)] = B &- \frac{2(A_1[(s)]^2 + B_1[(s)])}{D_1 + \sqrt{D_1^2 + 4C_1(A_1[(s)]^2 + B_1[(s)])}} \\ &- \frac{2(A_2[(s)]^2 + B_2[(s)])}{D_2 + \sqrt{D_2^2 + 4C_2(A_2[(s)]^2 + B_2[(s)])}} \\ &- \frac{2B_3[(s)]}{D_3 + \sqrt{D_3^2 + 4C_3B_3[(s)]}}\end{aligned} \tag{24}$$

After steady-state surface coverages are obtained, the entire system is integrated by one time step through a 4th-order Runge-Kutta scheme, to obtain product fluxes. The probability of a product is defined as the probability that an incoming reactant species ends up as a specific product. As examples, the probability of O_2 recombination through O-atom flux is given by Eq. (25), and the probability of N_2 recombination through N-atom flux is given by Eq. (26).

$$p_{O_2} = \frac{2f_{O_2}}{f_{O,in}} \tag{25}$$

$$p_{N_2} = \frac{2f_{N_2}}{f_{N.in}} \tag{26}$$

Furthermore, for reactions involving molecular oxygen, often the overall probability of O_2 oxidation is presented. In this case, we define the O_2 reaction probability by Eq. (27).

$$p_{O_2,reac} = \frac{2f_{CO_2} + f_{CO}}{2f_{O_2,in}} \tag{27}$$

In this manner, given the gas temperature, pressure, and species concentrations at the surface, the local flux of species to the surface is known and the ODEs can be solved for the resulting steady-state surface coverage and product fluxes, which we then present as probabilities. These probabilities of reaction outcomes are plotted over a wide range of temperature and pressure, and for various compositions such as pure O atoms, pure N atoms, and mixed O/N compositions. Results corresponding to molecular beam (MB) conditions are plotted by prescribing the temperature and pressure (arbitrarily) in order to recover the species flux in the actual molecular beam. It was also verified that integrating the equations in time to a steady-state (given an arbitrary initial surface coverage) matches precisely the solution obtained using the steady-state equations above. In the next section, we present model results along with the new continuous molecular beam data and other available data. While presenting comparisons between the model and experimental data, we provide explanation and justification for the choice of reaction mechanisms and model parameter values.

5. Comparison between model and experiment

Although the molecular beam experiments provide a wealth of data to construct the finite rate model, the effective pressure near the surface is very low. To be useful for hypersonic boundary layer conditions, the new model must be accurate over a large pressure range. Surface-coverage dependent models naturally introduce pressure dependence [31], and do so in a physically accurate manner through a balance between incident flux, adsorption, desorption, and product formation. It is not possible for such a finite-rate model to match all experimental data points, which, in the current study, span approximately 5 orders of magnitude in pressure and 2000 K in temperature. Furthermore, the model is further constrained when mixtures of O and N atoms are present, as these species compete for active surface sites. Therefore, the purpose of the new model is not to reproduce each experimentally inferred value precisely; rather the aim is to reproduce all of the measured trends in temperature and pressure, as well as the approximate magnitude of the reaction probabilities by a set of physics-based reaction mechanisms. While one could curve-fit the experimental data points, it is important to realize that the experimentally inferred values have uncertainty and that there is not enough data available. By constructing a physics-based model, the aim is that when it is extended to conditions between available experiments that the model is predictive and can guide future, more-targeted, experiments.

5.1. Reactions involving atomic oxygen (O) - Molecular beam conditions

Figure 1 shows the model predictions for a range of surface temperatures with atomic oxygen flux conditions representative of the new contin-

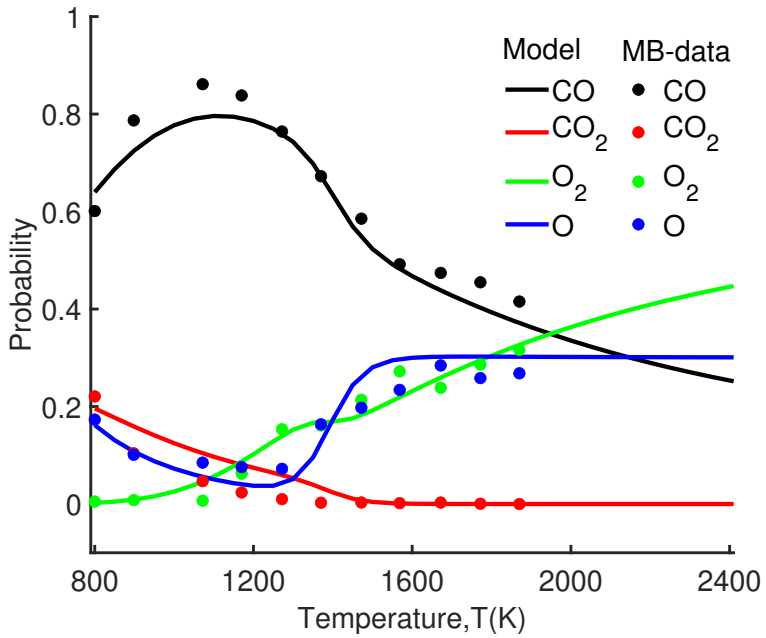

Figure 1: Model predictions vs molecular beam experimental data for O-atom reactions with carbon.

uous molecular beam experiments (5×10^{20} atoms m^{-2} s^{-1}) and compares with the probabilities inferred from the molecular beam experiments (described in Ref. [23]). While the model does not go through all data points, the major experimental trends are reproduced. As seen in Fig. 1, CO is the major reaction product and exhibits non-Arrhenius behavior as the surface temperature is increased. This is explained by the probability of O-atom removal from the surface, which has the opposite trend of CO production, and is also explained by the surface coverage trends shown in Fig. 2. At low temperatures, the surface has more than 10% total coverage and CO production increases with increasing temperature via reactions (3) and (7), which have identical Arrhenius expressions with the activation energy chosen

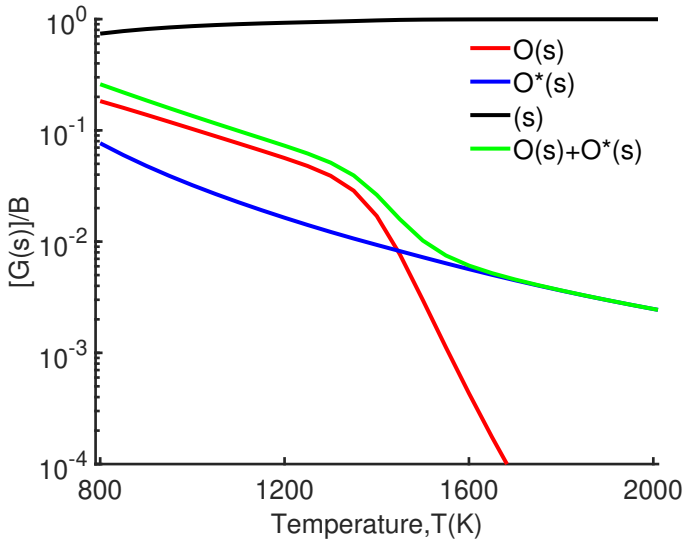

Figure 2: Surface coverage as a function of temperature predicted by the model for O-atom reactions with carbon.

to match the slope of increasing CO probability seen in the beam experiments at low temperatures. As the temperature approaches 1300 K, O(s) begins to rapidly desorb due to the single-bond desorption energy and the T^2 dependence of the transition state theory expression in reaction (2). This desorption is consistent with the increase in O scattering probability seen in the experimental points in Fig. 1 at the same temperature. Above this temperature, a low level of surface coverage is still maintained by O^*(s) due to the higher desorption energy that dominates over the T^2 dependence in reaction (6). This sustained surface coverage results in continued CO production at higher temperatures, as observed in the experiments. Note that in the previous oxygen-carbon model by Poovathingal et al. [21], only O(s) was included and a separate reaction was included to maintain CO production

at high temperatures. Poovathingal et al., noted that this reaction was not physically based and our new model shows that the correct high temperature trend is accurately captured by the introduction of $O^*(s)$. The pulsed molecular beam experiments exhibited a slowly decaying tail of product formation between beam pulses, which is evidence of a more strongly-bound adsorbed oxygen state [12]. Swaminathan-Gopalan et al. [27] introduced three types of adsorbed oxygen in order to model the transient reactivity between beam pulses.

A number of other experiments have observed a maximum in CO probability as the surface temperature is raised. For example, Figure 9.7 in the textbook "Nonequilibrium Hypersonic Aerothermodynamics" by Chul Park [32] shows several sets of experimental data for CO reaction probability due to atomic oxygen. Three experimental data sets (two sets from Rosner et al. and one set from Liu et al. [33][34]) show increasing CO probability as temperature is increased, but show clear maxima between 1200 K and 2000 K. In terms of finite-rate models for this reaction, the Park model [1] is a simple Arrhenius rate expression where CO probability monotonically increases with increasing temperature. In contrast, the recent surface-coverage based model by Swaminathan-Gopalan et al. [27] predicts the CO probability to *decrease* with increasing temperature above 700 K (for example, Fig. 9c in their paper [27] presents a comparison between several models). The previous model by Poovathingal et al. and the new air-carbon model developed in this article both predict increasing CO probability with increasing temperature until a maximum value is reached, consistent with available experimental data.

Figure 1 shows that CO_2 is a minor reaction product. At the lowest exper-

imental temperature (800 K), the CO_2 probability is a factor of three lower than the CO probability, and above 1000 K the measured CO_2 products become negligible. For simplicity we model CO_2 production as dependent only on O(s), which vanishes at high temperature, and we adjust the activation energy in reaction (4) to reproduce the decreasing slope of CO_2 probability observed in the molecular beam experiments.

The new continuous molecular beam experiments provided unique measurements of O-atom surface recombination on carbon. As seen in Fig. 1, the probability to form O_2 through recombination is effectively zero at 800 K and increases with temperature, reaching a non-negligible value of 0.3 at approximately 2000 K. We find that an LH mechanism for recombination (purely dependent on surface coverage) accurately captures the experimental trend. We include a separate LH mechanism for both types of adsorbed oxygen (O^*(s) and O(s)) in reactions (8) and (9). The activation energies are set to the same value, and the predicted trend matches the experimental slope of increasing probability with temperature. The inclusion of recombination reactions in the model adds considerable complexity, since recombination reactions deplete surface coverage and "compete" with CO production, especially at high temperatures. To control this competition at high temperatures where recombination is significant, the pre-exponential factor in reaction (8) (LH mechanism involving O^*(s)) is set to a different value than in reaction (9) (LH involving O(s)). This is purely a modeling choice, made to best reproduce the experimental trend. Finally, an expanded finite-rate model was tested that included ER-type mechanisms for oxygen surface recombination, however, they did not contribute to, or change the results of, the model. To

maintain model simplicity we do not include ER reactions for oxygen.

In reactions (1) and (5), the selectivities of adsorption to O(s) and O^*(s) are set to 0.3 and 0.7 respectively. While these values are somewhat arbitrary (no direct experimental evidence exists), a level of consistency is important for the model. The selectivities should add to unity, and in addition, the selectivities should be consistent with desorption behavior. For example, at 2000 K the desorption of O(s) is extremely rapid. If the selectivity of adsorption to O(s) was greater than 0.3 then, as result of rapid desorption, the probability of O atoms scattering off the surface would also be greater than 0.3. Since, in the high-temperature limit, the experimentally inferred probability (seen in Fig. 1) plateaus at approximately 0.3, we set the selectivity of adsorption to O(s) consistent with this value.

5.2. Reactions involving atomic oxygen (O) - High pressure conditions

The new model is entirely constructed based on the molecular beam data; however, because it includes surface-coverage dependence, it will also exhibit trends with pressure. Figure 3 shows model predictions for 0D simulations at a pressure of 5400 Pa, approximately equal to the highest partial pressure of O (at the surface) in air-ablation experiments performed in an ICP facility by Helber et al. [35]. The main trend, seen in Fig. 3 is that at high pressure surface coverage of O(s) is now maintained at higher temperatures and the peak in CO probability therefore shifts to a higher temperature. While the peak at molecular beam conditions occurred near 1100 K, the peak at 5400 Pa is closer to 1700 K. This shift is also seen in the O-atom scattering curve in Fig. 3, where the increase due to desorption is also delayed until 1700 K. At high pressure, the CO_2 probability increases slightly due to enhanced surface

coverage, however, remains low compared to the CO probability. The model predicts essentially no surface recombination to form O_2 at high pressure. The main reason for this trend is that the CO probability is sufficiently high (ranging between 0.7 and 0.9) that recombination reactions, which rely entirely on adsorbed O-atoms, cannot compete with CO production and O desorption.

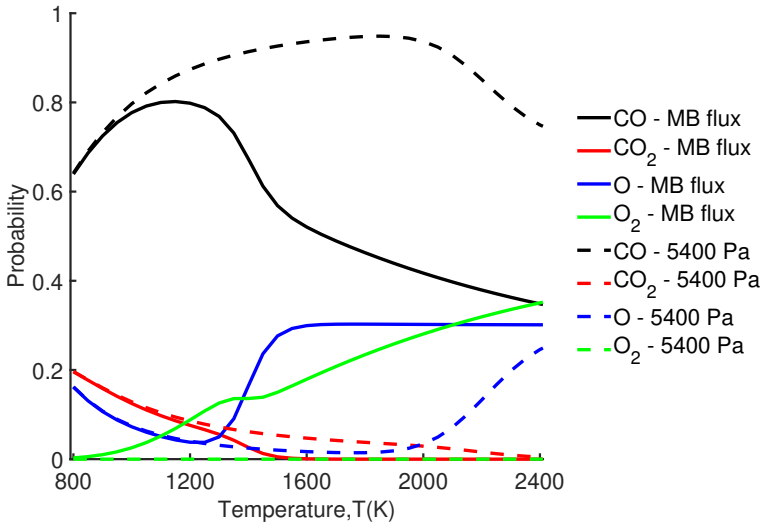

Figure 3: Model predictions for O-atom reactions at molecular beam conditions and at ICP conditions (P_O=5400 Pa).

It is important to note that the flux of species to the surface in plasma wind tunnel ablation tests is approximately 5 orders of magnitude larger than the flux in the molecular beam experiments. In order to maintain reasonable reaction probabilities over such a wide range of pressures (range of species flux), we find that including gas-phase dependence in the reaction mechanisms (i.e. reactions (3), (4), and (7)) is necessary. Such reaction mechanisms were used in the ZA model [2], the modifications proposed by

Maclean et al. [6], the modifications proposed by Alba et al. [10][11], and also in the previous molecular beam-based model of Poovathingal et al. [21]. This dependence ensures that if the flux of O atoms to the surface increases by orders of magnitude, then the overall rate of CO production increases proportionally. In contrast, if the CO reaction mechanism is dependent only on adsorbed species (for example O(s) + C(b) $\rightarrow$ CO + (s), similar to the mechanisms proposed by Swaminathan-Gopalan et al. [27]), then the CO reaction probability becomes very low at high pressure. The reason is that surface coverage remains relatively constant (typically between 0.05 and 0.2 in our model) with a maximum of unity, which limits the overall production rate of CO; the rate scales only with surface coverage rather than scaling with species flux. If the overall rate is limited due to high surface coverage at high pressure, yet the flux of species to the surface increases by orders of magnitude, the *probability* of CO formation will decrease by orders of magnitude. There is no evidence for such low probabilities of CO formation due to O-atoms at any pressure. For example, the Park model has a relatively constant CO probability with no pressure dependence, and the overall Park rate scales directly with incoming flux. To summarize, by including gas-phase dependence in reactions (3), (4), and (7) (and also in reactions (12), (17), (18), and (20) for other species) the product reaction rates scale with incoming flux and exhibit a moderate pressure dependence on the *probability* of each reaction. Specifically, our model predicts that the peak CO probability is shifted to higher temperature as pressure is increased as seen in Fig. 3.

Figure 4 compares the model behavior with the Park models [1] for the probability of CO production and O_2 production via recombination. While

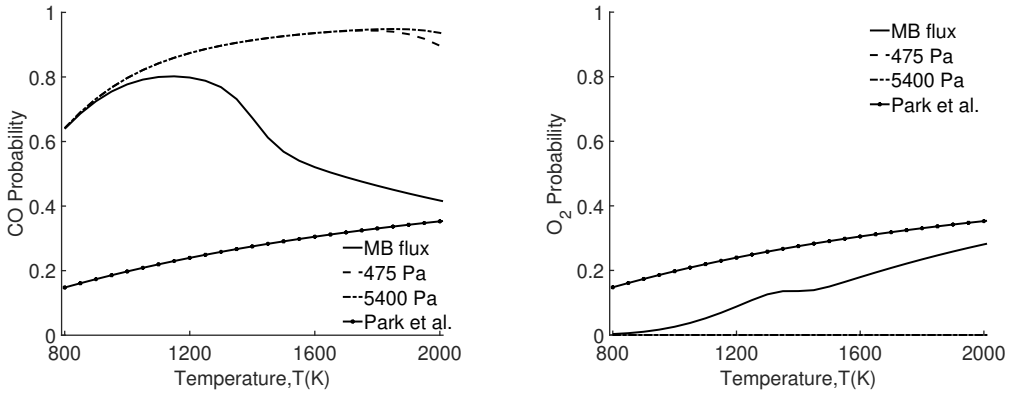

(a) CO (b) O_2

Figure 4: Model predictions at molecular beam flux conditions and at pressure conditions of 475 Pa and 5400 Pa compared to the Park model for (a) CO formation, and (b) O_2 recombination.

the Park model has no pressure dependence, the new model results are plotted for the molecular-beam flux conditions and two higher pressure conditions.

5.3. Reactions involving atomic nitrogen (N)

The new molecular beam experiments enable model extension to include CN production and N_2 production via surface recombination due to N atoms interacting with the VC surface. Figure 5 compares the model results to experimental data. Experimental data from the continuous molecular beam experiments [23] and results from ICP ablation experiments performed at the University of Vermont by Lutz and Fletcher [36] and at the von Karman Institute (VKI) for Fluid Dynamics by Helber et al. [37] are plotted in Fig. 5. The main trend is that the probability of recombination to form N_2 is approximately an order of magnitude larger than the probability of CN

formation in both the molecular beam experiments and in the ICP experiments by Lutz and Fletcher. Furthermore, the probability of CN formation is much lower than the probability of CO formation shown previously in Fig. 3. These are the main trends that the new model must capture.

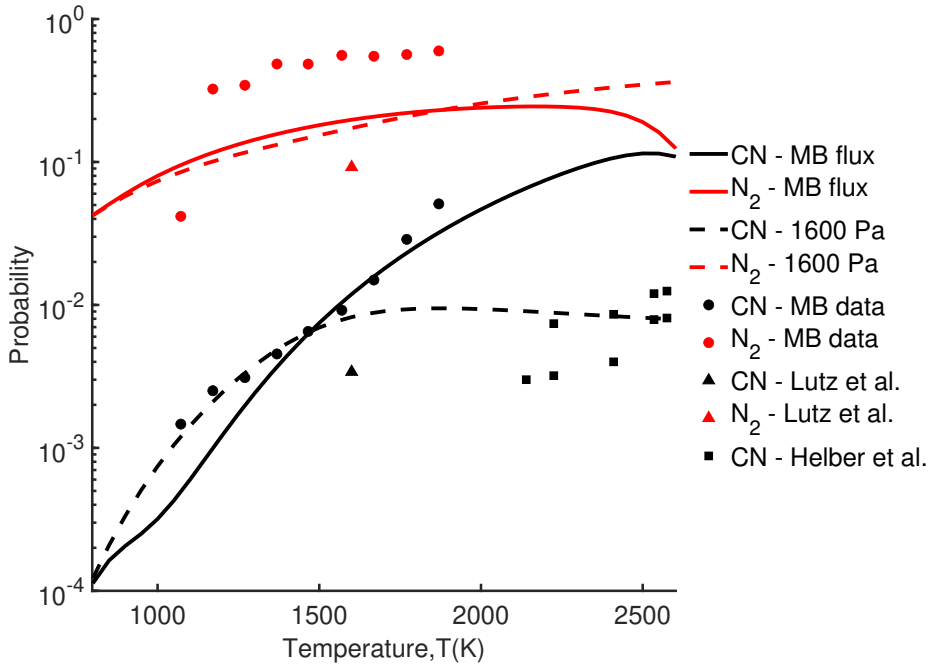

Figure 5: Model predictions compared to experimental data for N-atom reactions. Conditions correspond to molecular beam flux conditions [23] and the ICP experimental conditions from Lutz et al. [36] and Helber et al. [37] correspond to a pressure of 1600 Pa.

The molecular beam data shows a sharp drop in N_2 formation at low temperature, which could indicate that the adsorption energy of N atoms is sufficiently high (in magnitude) that N atoms are not very mobile until the temperature is increased [23]. Although there may be other ways to capture

this trend, we choose to model N-atom adsorption as an activated process, involving an energy barrier, by reaction (10). Further rationale for this choice is discussed in subsection 5.5, where competition between N and O atoms on the surface is analyzed.

The molecular beam data also shows no noticeable drop in reaction probability due to surface coverage loss up to 1800 K (the highest temperature tested), which could indicate that adsorbed N atoms, N(s), are more strongly bound to the surface than adsorbed O atoms. We find that a desorption energy larger than that corresponding to a single bond between C and N is required by the model. While the exact desorption energy cannot be deduced from the experimental data, we choose a desorption energy corresponding to a double bond between C and N in reaction (11). It is noted that, from a physical standpoint, this double-bond desorption energy may be high and not fully consistent with the molecular beam data, which indicates a lower energy barrier for CN formation. However, restricting the desorption energies for both oxygen and nitrogen to single and double bond values still enables the model to reproduce general experimental trends. Finally, unlike for oxygen, only a single "type" of adsorbed nitrogen is required to capture the experimental trends. Next, we model the production of CN using the same surface coverage dependent mechanism as used for CO production in reaction (12). Since this mechanism also includes dependence on the flux of N atoms, it contributes significantly under high pressure conditions. We therefore set the activation energy in reaction (12) to be consistent with the CN probabilities inferred from the ICP experiments. The model result for CN probability versus temperature, for a N-atom pressure of 1600 Pa (approximately equal

to the partial pressure of N atoms near the surface reported in the ICP experiments [36][37] is shown by the dotted black line in Fig. 5. This high pressure trend deviates from the CN probabilities inferred from the molecular beam experiments above 1500 K, which continue to rapidly increase with surface temperature. Although the reason for this apparent discrepancy between molecular beam and ICP experiments is not understood, it is postulated in Ref. [23] that this trend *"is consistent with a high-activation-energy step, such as chemisorption of N or cleavage of a C-CN bond from the surface"*, with the most likely scenario being C-CN bond cleavage. To capture this trend, such a bond-cleavage reaction mechanism is included in the model by reaction (15) where the activation energy is set to the value recommended by analysis of the molecular beam experiments [23]. The model results for CN probability under both high pressure conditions and molecular beam flux conditions are shown in Fig. 5. While both reaction mechanisms (12) and (15) contribute to the high pressure result, reaction (15) dominates the CN production when the flux to the surface becomes low, and the model is in reasonable agreement with both sets of experimental data.

Perhaps the most important aspect of the N-atom experiments is that the interactions are dominated by surface-catalyzed recombination into N_2 molecules, and that the reactions are essentially a competition between N_2 and CN formation. Because the model includes two mechanisms for CN formation, we also include two mechanisms for recombination; reaction (13) is an ER-type mechanism and reaction (14) is an LH-type mechanism. Although there was no evidence of ER-type recombination in the molecular beam experiments (near-vacuum conditions), both ER and LH reactions and

rate coefficients are chosen to give a high probability of recombination across a range of temperatures and pressures.

Finally, Fig. 6 compares CN formation probability predicted by the model, at both molecular beam flux conditions and also at high pressure ICP conditions, with available experimental data and with the Park model [1]. The Park model has no pressure dependence and predicts a very high CN formation probability compared to the experimental data, while the new model is constructed to accurately reproduce the experimental data.

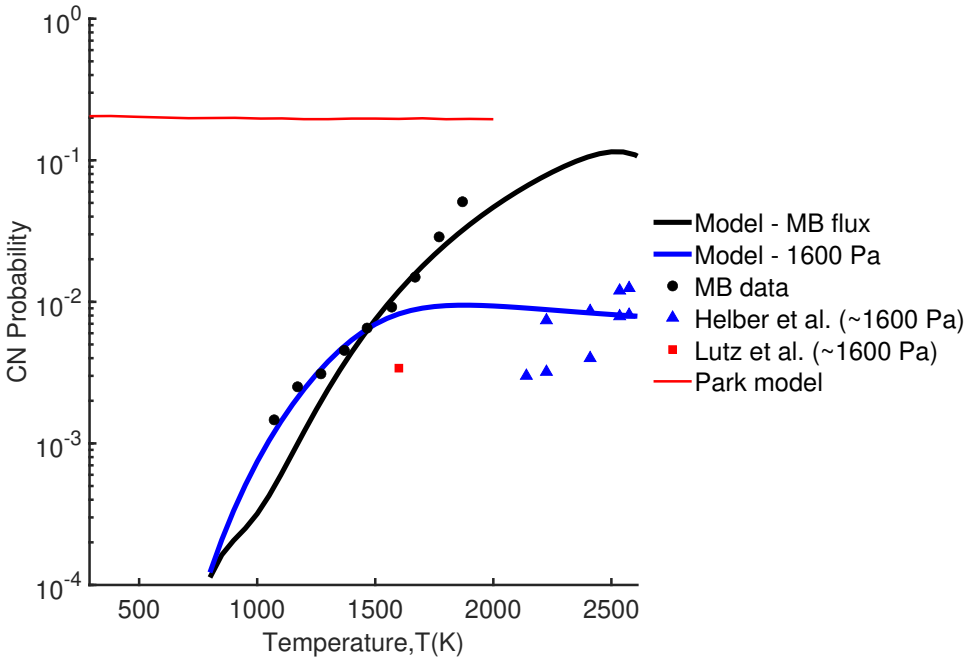

Figure 6: Model predictions for CN probability compared to the Park model and to experimental data.

5.4. Reactions involving molecular oxygen (O_2)

The reactivity of molecular oxygen with carbon is approximately between one and two orders of magnitude lower than that of atomic oxygen. For example, Figure 9.8 in the textbook "Nonequilibrium Hypersonic Aerothermodynamic" by Chul Park [32] shows several sets of experimental data for CO reaction probability due to molecular oxygen. In our model, the relative reactivity of molecular oxygen compared to atomic oxygen is entirely controlled by the adsorption mechanism for O_2. Specifically, in our model, molecular oxygen must dissociatively chemisorb on the surface (reactions (16) and (19)) and the energy barrier is set to reduce the reactivity of O_2 to levels observed in experiments. Other than the dissociative chemisorption process, once the dissociated oxygen atoms are adsorbed on the surface in either O(s) (reaction (16)) or O^*(s) (reaction (19)) states, the formation of CO and CO_2 proceeds via the same rates (i.e., the same mechanisms, pre-exponential factors, and activation energies) as the atomic-oxygen mechanisms as specificed by reactions (17), (18), and (20). Therefore, although the addition of molecular oxygen adds five reactions to the model, the only additional free parameter introduced is the activation energy for dissociative chemisorption.

With this simple dissociative chemisorption model, as seen in Fig. 7, the model shows good agreement with experimental data over a range of temperatures and pressures. Specifically, Fig. 7 shows the reactivity of O_2 with temperature as predicted by the model corresponding to recent molecular beam experimental conditions from Ross et al. [24], and two higher pressure experiments from Olander et al. [26] and Rosner et al. [25]. The experiments report the overall reactivity of O_2, combining both CO and CO_2 formation,

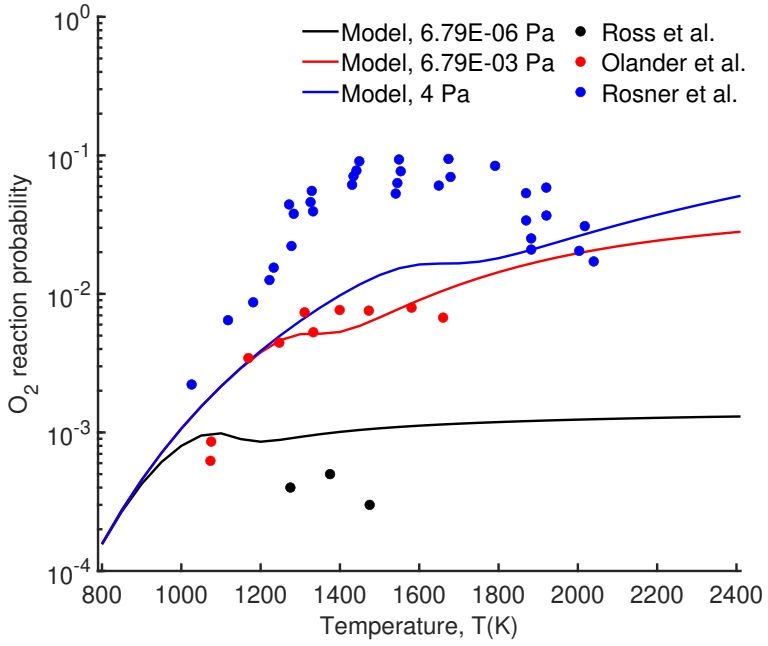

Figure 7: Model predictions compared to experimental data for O_2 reactivity to form CO and CO_2 products. The data from Ross et al. [24] corresponds to low molecular beam flux conditions, the data from Olander et al. [26] corresponds to a pressure of 6.79×10^{-3} Pa, and the data from Rosner et al. [25] corresponds to a pressure of 4 Pa.

and the model results are presented using Eq. 27 for consistency. Clearly, the reactivity of O_2 is several orders of magnitude lower compared to the reactivity of O. The fact that the model inherently captures a pressure dependence, in approximate agreement with the data, is interesting. At very low flux conditions, the probability of adsorbed oxygen recombining to form O_2 is relatively high (refer to Fig. 3) and, because O_2 reactivity is always low, recombination competes with surface coverage and further limits O_2 reactivity to form CO and CO_2. At higher flux conditions (higher pressures), recombination becomes less competitive (again refer to Fig. 3), and O_2 reac-

tivity to form CO and CO_2 is able to increase. Since O_2 reactivity is generally low to begin with, this pressure effect is quite noticeable in the semi-log plot in Fig. 7.

In an extended version of the model, we included ER-type recombination reactions for O atoms to form O_2 and also included partial dissociative chemisorption reactions for O_2 (in order to maintain detailed balancing). However, the addition of these reactions had little-to-no effect on model predictions at any temperature and pressure tested. In order to avoid unnecessary model complexity, these reactions were omitted from the final model. Finally, while the experimental data in Fig. 7 appears to show a similar maximum reaction probability, as observed for O-atom reactions, the trend is not as prominent. Also, since the amount of O_2 reactant flux to the surface may be low at these temperatures, combined with the low reactivity of O_2 on the surface, our simple model extension for O_2 reactions is appropriate.

5.5. Reactions in the presence of a mixture of atomic oxygen (O) and nitrogen (N)

One crucial aspect of constructing a surface-coverage dependent model that involves multiple species is understanding how these species may or may not compete for active sites on the material surface. For example, if N atoms are more strongly bound to the surface compared to O atoms (as in the current model), it may be possible that N atoms could block active sites and significantly reduce oxidation reactions. During the present joint computational-experimental study it became clear that this question needed to be addressed. For this reason, molecular beam experiments were performed using a mixed beam with both N and O atoms [22]. The results

indicated that there was no noticeable reduction in O-atom reactivity due to the presence of N atoms for for surface temperatures in the range 1100 - 1700 K. In fact, the experiments indicated that the presence of N atoms resulted in a slight *increase* in the O-atom reactivity. Therefore, our model is constructed in order to minimize competition between N and O atoms on the surface, such that the reaction trends for O and N remain relatively unchanged from the pure O-atom and pure N-atom results presented in previous sections.

One simple way to enforce no competition for surface sites between various species is to designate different surface sites for different species, for example (s_N) and (s_O) with corresponding total number of active sites B_N and B_O. Each species could then be constrained to adsorb on to, desorb, and react from, only their specific surface sites. While this strategy may be a convenient modeling assumption, a more realistic model should allow for competition between species.

The new model includes only one type of active surface site and therefore competition between O and N for surface sites is naturally predicted. To study the effect of N atoms on the oxidation rate to form CO (the dominant reaction), 0D simulations were performed for beam flux conditions with a composition of 50% O and 50% N. In the process of such testing we found that the activated adsorption process for N atoms (reaction (10)) has a significant effect on the mixture results. Figure 8a shows the CO probability results corresponding to a mixed beam with, and without, an activated adsorption process compared to the CO probability for a pure O-atom beam. If adsorption is not activated (no activation energy causing N adsorption to

be prompt like O), then because N atoms have a higher desorption energy, they accumulate and block surface sites. This effect is especially dominant at lower temperatures where CN and N_2 reactions are slow and do not "free-up" surface sites.

The blockage of surface sites by N atoms at low temperatures can be seen in Fig. 9. Figure 9b shows the surface coverage trends for a pure O-atom beam and Fig. 9c shows the trends for a mixed beam without an activated adsorption process. At low temperature, the N(s) is near unity and O-atom coverage is significantly reduced compared to the pure O-atom beam. With reactive sites blocked by N, the oxidation reaction probabilities drop considerably; the CO probability approaches zero at 800 K in Fig. 8a. If the adsorption of N atoms is modeled as an activated process, then at low temperatures N(s) is reduced, becoming comparable to the total O-atom coverage (as seen in Fig. 9a), which causes the CO probability to reduce by only a maximum of 30% at the lowest temperature (800 K). Given that the preliminary mixed O/N-atom beam data [22] shows no evidence of any reduction in CO probability due to the presence of N atoms, modeling N adsorption as an activated process as specified by reaction (10) helps reproduce this general result.

Figures 8b and 8c show the model predictions for a mixture of 50% O and 50% N at two higher pressure conditions. At higher pressures surface coverage is increased and more competition between O and N atoms on the surface results, since the total number of surface sites, B, remains fixed. At these higher pressures, the model predicts a 30% - 50% drop in CO reaction probability across the entire temperature range. If N adsorption is modeled

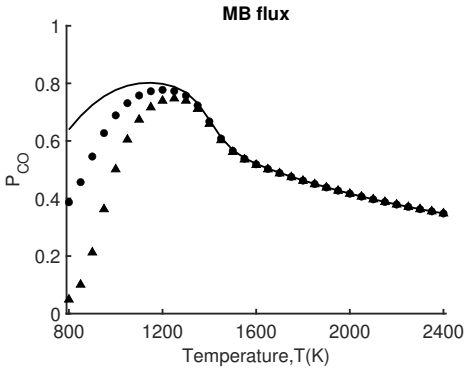

(a) Molecular beam flux conditions

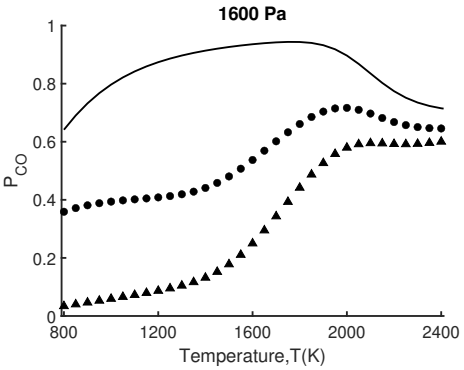

(b) Pressure equal to 1600 Pa

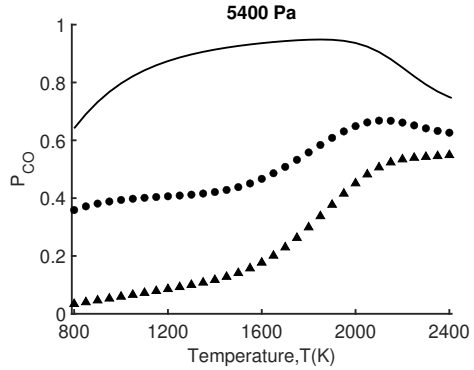

(c) Pressure equal to 5400 Pa

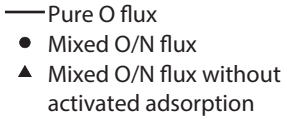

Figure 8: Model predictions for CO probability in a beam containing pure O, a mixed beam containing N and O at a flux ratio of 1:1, and a mixed beam containing N and O at a flux ratio of 1:1 without activated N adsorption at partial pressures of (a)2.4e-02 Pa, (b) 1600 Pa, and (c)5400 Pa.

as prompt (not activated), the CO probability drops by more than an order of magnitude for temperatures below 1600 K. Again, this indicates that N adsorption should be modeled as an activated process.

Therefore, the current model predicts only moderate competition effects at low flux conditions, in qualitative agreement with the mixed O/N molecular beam experiments [22]. However, at higher pressure conditions, competition effects between N and O atoms on the surface are predicted. Since the model will mainly be used for such higher pressure conditions, when N atoms are present near the surface, the CO reaction probability is predicted to resemble the trends seen in Figs. 8b and 8c (corresponding to the activated N adsorption process) with probabilities ranging approximately between 0.4 and 0.6. The competition for surface sites between different species, and the effect on reaction probabilities is perhaps the most complex aspect of a surface-coverage dependent model and further numerical and experimental studies are warranted. Furthermore, the experiments did not investigate surface recombination of N and O atoms into NO molecules. If this is verified to be a dominant reaction at high pressure conditions, the model could be expanded to include such reactions in future work.

6. Conclusions

Recent molecular beam experiments of high velocity O, N, and O_2 species impacting carbon material heated to high temperature, have produced a wealth of detailed surface chemistry data relevant for carbon ablation processes. New data has been obtained using a continuous molecular beam with lower velocity (2000 m/s) and approximately 500 times higher beam flux than

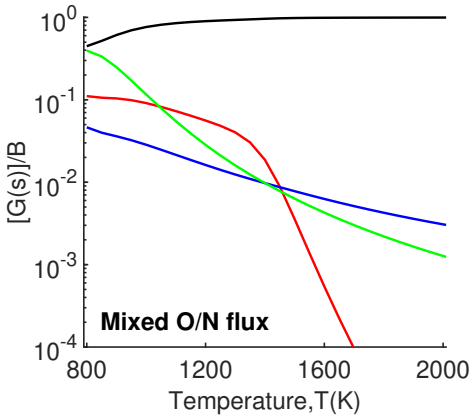

(a) Mixed O/N

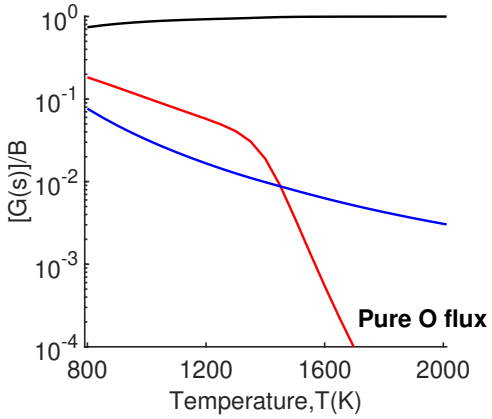

(b) Only O

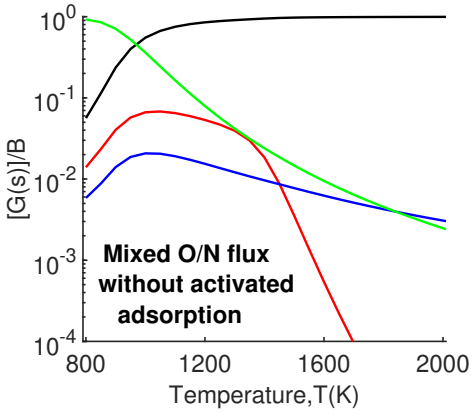

(c) Mixed O/N without activated adsorption

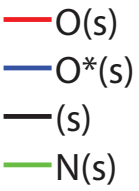

Figure 9: Surface coverage as predicted by the model in three cases - a) a mixed beam containing N and O each at 2.4e-02 Pa, with activated adsorption for N, b) a beam containing only O at 2.4e-02 Pa, c) a mixed beam containing N and O each at 2.4e-02 Pa, without activated adsorption for N atoms.

previous pulsed beam experiments. This experimental data is interpreted to construct a new air-carbon ablation model for use in hypersonic flight modeling involving carbon heat shield ablation. The new model is a finite-rate model where gas-surface reactions are dependent on the surface coverage of adsorbed O and N atoms. The new model comprises 20 reaction mechanisms describing reactions between impinging O, N, and O_2 species and producing scattered products including desorbed O and N atoms, O_2 and N_2 molecules formed by surface-catalyzed recombination, as well as CO, CO_2, and CN reaction products. Impinging N_2 molecules are modeled as being inert. The new surface-coverage dependent rate model exhibits non-Arrhenius reaction probability behavior in agreement with the molecular beam and other experimental observations.

All reaction mechanisms and reaction rate coefficients (selectivities, pre-exponential factors, and activation energies) are described in detail and each is supported by experimental evidence. Such modeling research would not be possible without the unique capability of molecular beam facilities to study individual gas-surface interactions, in contrast to high-enthalpy ablation test facilities where measurements are the net result of many reaction processes. The new model is constructed almost entirely based on molecular beam data, which involves very low flux conditions, several orders of magnitude lower than the expected flux in a hypersonic boundary layer. However, since the model is surface-coverage dependent it naturally predicts pressure effects and is tested for a wide range of temperatures and pressures relevant to hypersonic flight conditions.

The main trends produced by the new air-ablation model include: (i) CO

is the dominant reaction product with probabilities ranging from 0.4 to 0.8, (ii) CO_2 is a minor reaction product especially above surface temperatures of 1000 K, (iii) recombination of O atoms into O_2 molecules is predicted at very low flux conditions but becomes negligible at moderate to high pressure conditions, (iv) the probability of N-atom recombination into N_2 molecules is approximately 0.1, which is 10 times higher than the probability of CN formation, (v) the probability of CN formation is approximately 0.01, which is 100 times lower than CO production, except under very low flux molecular beam conditions where the probability of forming CN rises as high as 0.1, (vi) the reactivity of O_2 molecules to form CO and CO_2 is relatively small, ranging from 0.001 to 0.1 and exhibiting strong pressure dependence, (vii) all reaction products (except CO_2) have non-Arrhenius behavior where reaction probabilities increase with increasing surface temperature; however at high temperatures the probability of reaction either plateaus or begins to decrease due to loss of surface coverage. All of these main trends are shown to be in agreement with data from molecular beam facilities and also with limited data from inductively coupled plasma (ICP) wind tunnel facilities.

The new model has significant differences compared to the Zhluktov and Abe (ZA) model [2], the most notable of which is that the ZA model predicts the dominant reaction product to be CO_2 as discussed in prior research [21]. The new model also has significant differences compared to the recent model from Swaminathan-Gopalan et al., which was constructed based on pulsed molecular beam experimental data. The key difference is that, over the temperature range studied, the model of Swaminathan-Gopalan [27] predicts that the probability of CO formation always *decreases* with increasing

surface temperature. Finally, the new model predicts a similar probability trend for CO formation as the Park model [1] but a dramatically different trend for CN production. Furthermore, the purpose of the new model is to introduce surface-coverage dependence (pressure dependence) and non-Arrhenius behavior that the Park model does not attempt to capture. The new model builds on the previous oxygen-carbon model of Poovathingal et al. [21] by incorporating the wealth of new molecular beam data for new species and enables the simulation of dissociated air reacting with high temperature carbon.

The new air-carbon ablation model is considerably more complex than previous models that involved only O-atom reactions with carbon. There are a number of effects predicted by the model that have no supporting experimental evidence at this time, for example the prediction that at moderate to high pressures N atoms may compete with O atoms for surface coverage and reduce the CO production by 30% - 50% compared to pure oxygen conditions. Additionally, the model does not include recombination of O and N atoms to form NO molecules, as this reaction was not studied in the molecular beam experiments. Ultimately, the model requires validation within CFD simulations of high-enthalpy ablation experiments. For example, the probabilities of CO formation and N_2 recombination are quite high and it is possible that with new experimental data in high-enthalpy facilities that such magnitudes may need adjustment. However, the new model formulation and its ability to capture pressure and temperature dependence through fundamental reaction mechanisms can serve as a baseline model for ablation researchers to continually improve for specific applications.

When validating or modifying a finite-rate ablation model based on an experiment, it is extremely important that the experimental environment is well-characterized, including the freestream flow state and ultimately the near-surface gas state. If the local flux of reactant species to the carbon surface is specified inaccurately, and is not truly representative of the actual flux in the experiment, then the air-carbon ablation model should not be expected to agree with the measured recession rate or surface heat flux.

Acknowledgments

This work was sponsored by the U.S. Air Force Office of Scientific Research (AFOSR) under grant FA9550-17-1-0057. The views and conclusions contained herein are those of the authors and should not be interpreted as necessarily representing the official policies or endorsements, either expressed or implied, of the AFOSR or the U.S. Government.

References

[1] C. Park, Effects of atomic oxygen on graphite ablation, AIAA J. 14 (11) (1976) 1640–1642. doi:10.2514/3.7267.

[2] S. V. Zhluktov, T. Abe, Viscous shock-layer simulation of airflow past ablating blunt body with carbon surface, J. Thermophys. Heat Trans. 13 (1) (1999) 50–59. doi:10.2514/2.6400.

[3] M. A. Havstad, R. M. Ferencz, Comparison of surface chemical kinetic models for ablative reentry of graphite, J. Thermophys. Heat Trans. 16 (4) (2002) 508–515. doi:10.2514/2.6725.

[4] M. R. Wool, Passive nosetip technology (pant) program, Acurex Corp., Aerotherm Division Final Summary (June 1975) Rept. 75–159.

[5] R. Gosse, G. Candler, Evaluation of carbon-carbon ablation models using a fully coupled cfd solver, in: 40th Thermophysics Conference, 2008, p. 3908.

[6] M. MacLean, J. Marschall, D. Driver, Finite-rate surface chemistry model, ii: Coupling to viscous navier-stokes code, in: 42nd AIAA Thermophysics Conference, 2011, p. 3784.

[7] G. Candler, Nonequilibrium processes in hypervelocity flows: an analysis of carbon ablation models, in: 50th AIAA Aerospace Sciences Meeting including the New Horizons Forum and Aerospace Exposition, 2012, p. 724.

[8] S. W. Lewis, R. G. Morgan, T. J. McIntyre, C. R. Alba, R. B. Greendyke, Expansion tunnel experiments of earth reentry flow with surface ablation, J. Spacecraft Rockets 53 (5) (2016) 887–899. doi:10.2514/1.A33267.

[9] S. W. Lewis, R. G. Morgan, T. J. Mcintyre, C. Alba, R. B. Greendyke, Comparison of carbon ablative shock-layer radiation with high surface temperatures, in: 45th AIAA Thermophysics Conference, 2015, p. 2348.

[10] C. R. Alba, R. B. Greendyke, S. W. Lewis, R. G. Morgan, T. J. McIntyre, Numerical modeling of earth reentry flow with surface ablation, J. Spacecraft Rockets 53 (1) (2016) 84–97. doi:10.2514/1.A33266.

[11] C. R. Alba, R. B. Greendyke, J. Marschall, Development of a nonequilibrium finite-rate ablation model for radiating earth reentry flows, J. Spacecraft Rockets 53 (1) (2016) 98–120. doi:10.2514/1.A33303.

[12] V. J. Murray, B. C. Marshall, P. J. Woodburn, T. K. Minton, Inelastic and reactive scattering dynamics of hyperthermal o and o2 on hot vitreous carbon surfaces, J. Phys. Chem. C 119 (26) (2015) 14780–14796. doi:10.1021/acs.jpcc.5b00924.

[13] V. J. Murray, T. K. Minton, Gas-surface interactions of atomic nitrogen with vitreous carbon, Carbon 150 (2019) 85–92. doi:https://doi.org/10.1016/j.carbon.2019.04.117.

[14] D. J. Garton, T. K. Minton, B. Maiti, D. Troya, G. C. Schatz, A crossed molecular beams study of the o(3p)+h2 reaction: Comparison of excitation function with accurate quantum reactive scattering calculations, J. Chem. Phys. 118 (4) (2003) 1585–1588. doi:10.1063/1.1539043.

[15] D. Troya, G. C. Schatz, Theoretical studies of hyperthermal o(3p) collisions with hydrocarbon self-assembled monolayers, J. Chem. Phys. 120 (16) (2004) 7696–7707. doi:10.1063/1.1688312.

[16] D. J. Garton, A. L. Brunsvold, T. K. Minton, D. Troya, B. Maiti, G. C. Schatz, Experimental and theoretical investigations of the inelastic and reactive scattering dynamics of o(3p) + d2, J. Phys. Chem. A 110 (4) (2006) 1327–1341, pMID: 16435793. doi:10.1021/jp054053k.

[17] J. Zhang, D. J. Garton, T. K. Minton, Reactive and inelastic scattering dynamics of hyperthermal oxygen atoms on a saturated

hydrocarbon surface, J. Chem. Phys. 117 (13) (2002) 6239–6251. doi:10.1063/1.1460858.

[18] V. J. Murray, E. J. Smoll, T. K. Minton, Dynamics of graphite oxidation at high temperature, J. Phys. Chem. C 122 (12) (2018) 6602–6617. doi:10.1021/acs.jpcc.7b11772.

[19] S. J. Poovathingal, M. Qian, V. J. Murray, T. K. Minton, Reactive and scattering dynamics of hyperthermal o and o2 from a carbon fiber network, https://scholarworks.montana.edu/xmlui/handle/1/14696 (2018).

[20] S. Poovathingal, T. E. Schwartzentruber, V. J. Murray, T. K. Minton, Molecular simulation of carbon ablation using beam experiments and resolved microstructure, AIAA J. 54 (3) (2016) 999–1010. doi:10.2514/1.J054562.

[21] S. Poovathingal, T. E. Schwartzentruber, V. J. Murray, T. K. Minton, G. V. Candler, Finite-rate oxidation model for carbon surfaces from molecular beam experiments, AIAA J. 55 (5) (2017) 1644–1658. doi:10.2514/1.J055371.

[22] X. Chenbiao, T. K. Minton, Effect of n atoms on o-atom reactivity with carbon, ChemRxiv. Preprint. https://doi.org/10.26434/chemrxiv.12510716.v1 (2020).

[23] V. J. Murray, P. Recio, A. Caracciolo, C. Miossec, N. Balucani, P. Casavecchia, T. K. Minton, Oxidation and nitridation of vitre-

ous carbon at high temperatures, Carbon 167 (2020) 388 – 402. doi:https://doi.org/10.1016/j.carbon.2020.05.076.

[24] R. Edel, T. Grabnic, B. Wiggins, S. J. Sibener, Atomically-resolved oxidative erosion and ablation of basal plane hopg graphite using supersonic beams of o_2 with scanning tunneling microscopy visualization, J. Phys. Chem. C 122 (26) (2018) 14706–14713. doi:10.1021/acs.jpcc.8b04139.

[25] D. Rosner, H. Allendorf, High temperature oxidation of carbon by atomic oxygen, Carbon 3 (2) (1965) 153–156. doi:https://doi.org/10.1016/0008-6223(65)90042-4.

[26] D. Olander, R. Jones, J. Schwarz, W. Siekhaus, Reactions of modulated molecular beams with pyrolytic graphite. ii. oxidation of the prism plane, J. Chem. Phys. 57 (1972) 421. doi:10.1063/1.1677981.

[27] K. Swaminathan-Gopalan, A. Borner, V. J. Murray, S. Poovathingal, T. K. Minton, N. Mansour, K. A. Stephani, Development and validation of a finite-rate model for carbon oxidation by atomic oxygen, Carbon 137 (2018) 313–332. doi:https://doi.org/10.1016/j.carbon.2018.04.088.

[28] K. Swaminathan-Gopalan, K. A. Stephani, Construction of finite rate surface chemistry models from pulsed hyperthermal beam experimental data, AIP Adv. 9 (2019) 035246. doi:10.1063/1.5082553.

[29] R. Nieman, B. Jayee, T. Minton, W. Hase, H. Guo, Exploring reactivity and product formation in n(4s) collisions with pristine and defected graphene with direct dynamics simulations, Submitted to J. Chem.

[30] J. Marschall, M. MacLean, P. E. Norman, T. E. Schwartzentruber, Nonequilibrium flows: Fundamentals and recent advances, chapter 6: Surface chemistry in nonequilibrium flows, AIAA Progress in Astronautics and Aeronautics (2015).

[31] C. Sorensen, P. Valentini, T. E. Schwartzentruber, Uncertainty analysis of reaction rates in a finite rate surface catalysis model, J. Thermophys. Heat Trans. 26 (3) (2012) 407–416. doi:10.2514/1.T3823.

[32] C. Park, Nonequilibrium hypersonic aerothermodynamics, John Wiley and Sons, New York (1989).

[33] D. E. Rosner, H. D. Allendorf, Comparative studies of the attack of pyrolytic and isotropic graphite by atomic and molecular oxygen at high temperatures., AIAA J. 6 (4) (1968) 650–654. doi:10.2514/3.4558.

[34] G. N.-K. Liu, High temperature oxidation of graphite by a dissociated oxygen beam, Tech. Rep. MIT-TR-186, Massachusetts Institute of Technology Department of Aeronautics and Astronautics Aerophysics Laboratory (Aug 1973).

[35] B. Helber, O. Chazot, A. Hubin, T. E. Magin, Microstructure and gas-surface interaction studies of a low-density carbon-bonded carbon fiber composite in atmospheric entry plasmas, Compos. Part A Appl. Sci. Manuf. 72 (2015) 96 – 107. doi:https://doi.org/10.1016/j.compositesa.2015.02.004.

[36] A. Lutz, Experimental investigation and analysis of high-enthalpy nitrogen flow over graphite, PhD Thesis (2015).

[37] B. Helber, A. Turchi, T. E. Magin, Determination of active nitridation reaction efficiency of graphite in inductively coupled plasma flows, Carbon 125 (2017) 582–594. doi:https://doi.org/10.1016/j.carbon.2017.09.081.